ISSN 1674-1056
http://cpb.iphy.ac.cn
http://iopscience.iop.org/cpb
中国物理 B
Chinese Physics
中国物理
Chinese Physics B

Influence of fluoroethylene carbonate on the solid electrolyte interphase of silicon anode for Li-ion batteries: A scanning force spectroscopy study

Jieyun Zheng(郑杰允), Jialiang Liu(刘家亮), Suijun Wang(王绥军), Fei Luo(罗飞), Liubin Ben(贲留斌), Hong Li(李泓)

Citation: Chin. Phys. B . 2020, 29(4): 048203 . **doi:** 10.1088/1674-1056/ab7b54
Journal homepage: http://cpb.iphy.ac.cn; http://iopscience.iop.org/cpb

What follows is a list of articles you may be interested in

Failure analysis with a focus on thermal aspect towards developing safer Na-ion batteries

Yuqi Li(李钰琦), Yaxiang Lu(陆雅翔), Liquan Chen(陈立泉), Yong-Sheng Hu(胡勇胜)

Chin. Phys. B . 2020, 29(4): 048201 . **doi:** 10.1088/1674-1056/ab7906

Computational screening of doping schemes for$LiTi_2(PO_4)_3$ as cathode coating materials

Yu-Qi Wang(王宇琦), Xiao-Rui Sun(孙晓瑞), Rui-Juan Xiao(肖睿娟), Li-Quan Chen(陈立泉)

Chin. Phys. B . 2020, 29(3): 038202 . **doi:** 10.1088/1674-1056/ab7186

Theoretical study on the relationship between the position of the substituent and the ESIPT fluorescence characteristic of HPIP

Xin Zhang(张馨), Jian-Hui Han(韩建慧), You Li(李尤), Chao-Fan Sun(孙朝范), Xing Su(苏醒), Ying Shi(石英), Hang Yin(尹航)

Chin. Phys. B . 2020, 29(3): 038201 . **doi:** 10.1088/1674-1056/ab6d50

The n-type Si-based materials applied on the front surface of IBC-SHJ solar cells

Jianhui Bao(包建辉), Ke Tao(陶科), Yiren Lin(林苡任), Rui Jia(贾锐), Aimin Liu(刘爱民)

Chin. Phys. B . 2019, 28(9): 098201 . **doi:** 10.1088/1674-1056/ab33ec

Structural and dielectric properties of giant dielectric $Na_{1/2}Sm_{1/2}Cu_3Ti_4O_{12}$ ceramics prepared by reactive sintering methods

H Mahfoz Kotb

Chin. Phys. B . 2019, 28(9): 098202 . **doi:** 10.1088/1674-1056/ab37f1

SPECIAL TOPIC — Advanced calculation & characterization of energy storage materials & devices at multiple scale

Influence of fluoroethylene carbonate on the solid electrolyte interphase of silicon anode for Li-ion batteries: A scanning force spectroscopy study*

Jieyun Zheng(郑杰允)[1], Jialiang Liu(刘家亮)[2], Suijun Wang(王绥军)[2], Fei Luo(罗飞)[1], Liubin Ben(贲留斌)[1], and Hong Li(李泓)[1,†]

[1] *Beijing National Laboratory for Condensed Matter Physics, Institute of Physics, Chinese Academy of Sciences, Beijing* 100190, *China*
[2] *State Key Laboratory of Operation and Control of Renewable Energy & Storage Systems, China Electric Power Research Institute, Beijing* 100192, *China*

(Received 30 December 2019; revised manuscript received 26 February 2020; accepted manuscript online 1 March 2020)

Silicon is an important high capacity anode material for the next generation Li-ion batteries. The electrochemical performances of the Si anode are influenced strongly by the properties of the solid electrolyte interphase (SEI). It is well known that the addition of flouroethylene carbonate (FEC) in the carbonate electrolyte is helpful to improve the cyclic performance of the Si anode. The possible origin is suggested to relate to the modification of the SEI. However, detailed information is still absent. In this work, the structural and mechanical properties of the SEI on Si thin film anode in the ethylene-carbonate-based (EC-based) and FEC-based electrolytes at different discharging and charging states have been investigated using a scanning atomic force microscopy force spectroscopy (AFMFS) method. Single-layered, double-layered, and multi-layered SEI structures with various Young's moduli have been visualized three dimensionally at nanoscale based on the hundreds of force curves in certain scanned area. The coverage of the SEI can be obtained quantitatively from the two-dimensional (2D) project plots. The related analysis indicates that more soft SEI layers are covered on the Si anode, and this could explain the benefits of the FEC additive.

Keywords: Si, fluoroethylene carbonate, solid electrolyte interphase, atomic force microscopy force spectroscopy

PACS: 82.47.Aa, 82.45.Fk, 79.60.Jv, 68.37.Ps **DOI:** 10.1088/1674-1056/ab7b54

1. Introduction

Non-aqueous liquid electrolytes are widely used in commercial Li-ion batteries for portable electronics, electric vehicles, and many other applications.[1–3] Electrolytes with high conductivity, safety, and compatibility with the electrodes are desirable.[4] It is favorable but not necessary that the electrolyte should keep electrochemically stable in a wide electrochemical window. If the exposed surface of cathode and anode towards the electrolyte can be covered by a stable passivating layer, the battery can also operate well. Such a passivating layer is well known and called the solid electrolyte interphase (SEI).[5] The SEI plays a critical role in determining the Coulumbic efficiency, cycle life, calendar life, rate performance, energy efficiency, gas release, self-discharge, and safety for Li-ion batteries.[6–9] Based on experimental investigations using x-ray photoelectron spectroscopy (XPS),[10] electrochemical impedance spectra (EIS),[11] and secondary ion mass spectrometry (SIMS)[12] techniques, it is generally accepted that the SEI is composed of at least two layers. The inner layer is the inorganic layer, containing Li_2CO_3, Li_2O, LiF, and LiOH. The outer layer is the organic and polymer layer, containing LiOR, $ROCO_2Li$, and PEO-Li.[13,14] Such complicated multi-layered structure has been reconstructed by molecular dynamic (MD) simulation.[15] It is also known that the SEI is amorphous and the thickness ranges from 2 nm to hundreds of nanometers. Therefore, it is very difficult to detect the structure of the SEI experimentally.

Si is known as the most promising anode material for the next generation of Li-ion batteries due to its high specific capacity of 3579 $mA{\cdot}h{\cdot}g^{-1}$ associated with the formation of $Li_{15}Si_4$ at room temperature. It was noticed by the authors in 1999 that the capacity retention of Si can be improved by decreasing the particle size to nanometers.[16–18] However, the challenges of Si anodes are quite difficult to overcome. One is the large volume variation ($\sim$ 320% for fully discharge and charge) during the lithiation/delithiation process.[19–22] It leads to the pulverization of the Si materials with large particle size and worsen of the electrical connection between the electrode and the current collector. Another issue is the SEI film on Si anode. The chemical compositions of the SEI on Si anodes at different states upon cycling are explored by XPS, which are found similar with graphite anode such as Li_2CO_3, LiF, and Li-contained organic species. The SEI exhibits different morphology at different potential during the first two cycle as confirmed by scanning electronic microscopy (SEM).[23] It

*Project supported by the State Grid Technology Project, China (Grant No. DG71-17-010).
†Corresponding author. E-mail: hli@iphy.ac.cn
© 2020 Chinese Physical Society and IOP Publishing Ltd

was suggested that the SEI layer is mainly composed of inorganic species (LiF, LiP_xF_y, *et al.*) under high rate and organic carbonate species (alkyl lithium carbonates, *et al.*) under low rate, this phenomenon is confirmed by XPS and ToF-SIMS.[24]

A stable passivating layer with 100% coverage for the SEI film is expected. However, up to now, the quantitative information of the SEI coverage on electrodes in lithium batteries is difficult to obtain, including Si anodes. It is not clear (1) whether the Si anode is covered by the SEI film completely after the first cycle; (2) whether the SEI can maintain stable after large volume variation; (3) whether the reformation of the SEI film on the fresh exposed surface after the formation of cracks will lead to the worsen of the electronic contact.

In spite of the above uncertainties in the SEI film on Si anode, it has been found that the use of additives effectively improves the cyclic performances of Si and other anodes through modifying the SEI film.[25–28] And flouroethylene carbonate (FEC) has been widely used as additive[29–34] or co-solvent[35–41] of electrolyte for Si anodes. The enhancement of the cyclic performance is ascribed to the better properties of the FEC-induced SEI, such as smooth surface,[29,33] low impedance,[36,39] and protecting the Si anode from oxidation.[35] The detected chemical components of the SEI on Si anodes in FEC-contained electrolyte are LiF, oxalates, polyene-compounds, polycarbonate species, Si–F based products, *et al.* However, the detailed structure of the SEI, especially the mechanical properties and the coverage of the SEI are still not clear, which are key information for properly understanding the functions of the FEC.

Atomic force microscopy (AFM) has been used to study the SEI for a long time.[42] The thickness of the SEI on highly oriented pyrolytic graphite (HOPG) was 25 nm in a 1 μm×1 μm area measured by the AFM tip according to Kotz's results.[43] Chu found that the SEI formed at a higher potential on the edge surface of HOPG than on basal surface via an electrochemical AFM technique.[44] Micro-structural evolution process such as curling, swelling, and exfoliation of the HOPG particle caused by the intercalation of solved lithium ions was observed by Ogumi's group.[45] And this group has also found that the SEI can dissolve and agglomerate when stored at elevated temperature.[46]

The surface evolution of the Si-based anode material during cycling can be investigated through an AFM equipped inside the argon-filled glove box.[47] The volume change of the Si upon lithiation/delithiation was observed by several groups using AFM.[47–49] And the cracks of the Si thin film after cycle were also confirmed.[50] All these *in-situ* or *ex-situ* AFM studies are helpful for understanding the interface problems and designing lithium batteries with better performance. Recently, an AFM based method, force spectroscopy (AFMFS), has been proposed to study the SEI of the MnO thin film,[51] HOPG[52] anode for Li-ion batteries, and has also been extended to study the SEI of Na-ion batteries.[53] The deformation of the sample and the force acted on the tip are recorded during the repulsive interaction process between the sample and the tip. Consequently, the Young's modulus and the thickness of the SEI can be measured. This is quite helpful to obtain the mechanical property of the SEI film.

In this work, *ex situ* AFMFS method has been developed further by scanning the surface and collecting a large quantity of force curves. Accordingly to the analysis, the coverage, three-dimensional (3D) structure, and mechanical properties of the SEI on the Si anode can be obtained, which is helpful for understanding the function of the FEC and clarifying the problems listed above.

2. Experiment

2.1. Materials

Silicon nanopowder with an average size of 100 nm was purchased from Hefei Kaier Nanotechnology Development Co., Ltd. Super P carbon and sodium alginate were purchased from Sigma-Aldrich. All chemicals were used as received without further purification.

2.2. Electrode preparation and cell assembly

The 70 wt% silicon nanopowder, 15 wt% super P carbon, and 15 wt% sodium alginate in deionized water as solvent were mixed using a Germany IKA Eurostar 6000 stirrer (2000 rpm) for at least 10 h to obtain homogeneous slurries. Then, these slurries were coated on a Cu foil using a 100 μm doctor-blade. After coating, the film was dried in an air dry oven at 30 ℃ for 2 h, compressed under 1 MPa between two stainless steel plates, and cut into sheets with an area of 0.8 cm^2. The average mass loading of silicon was 2.34 mg/cm^2. These sheets were dried in a vacuum oven at 120 ℃ to remove the solvent. The silicon electrodes were obtained for electrochemical performance measurements.

The test cells were assembled into CR2032 cells with a metal lithium foil as the counter electrode and a Celgard separator in an argon-filled glove box. The electrolytes of the cells were made with: (i) 1 M $LiPF_6$ in EC/DMC (1 : 1, v/v), a commercially available electrolyte for lithium ion batteries, and (ii) 1 M $LiPF_6$ in FEC/DMC (3 : 7, v/v). The discharge and charge measurements were carried out on a Land BT2000 battery test system (Wuhan, China). All these cells were cycled between 10 mV and 1 V versus Li/Li^+ at a 0.05 C rate (210 $mA{\cdot}g^{-1}$) for the first cycle and a 0.2 C rate (840 $mA{\cdot}g^{-1}$) for subsequent cycles.

2.3. Elecrtrochemical testing

Electrochemical cycling of the assembled half-cell was performed by Arbin automatic cell tester between 2 V and

0.005 V at 0.2 C. Different electrochemical states are listed in Table 1. For the FEC-free sample, the cut-off voltages were 0.05 V, 0.005 V, and 0.005 V (kept at 0.005 V for 48 h) in the first discharging process, and 2 V was chosen in the charging process. With addition of 30% FEC in the electrolyte, the samples were discharged to 0.2 V (sample 6), 0.05 V (sample 7), 0.005 V (sample 8), and 0.005 V (sample 9) for 48 h. Sample 10 was charged to 2 V at room temperature after the first discharging process. Sample 11 was discharged to 0.005 V and kept at 0.005 V (55 ℃) for 48 h. Sample 12 was charged to 2 V.

Table 1. Different cycle stages of silicon thin films.

Sample No.	Electrochemical states (cut-off voltage)	Electrolyte & temperature
Sample 1	pristine silicon,	EC-based electrolyte, RT
Sample 2	discharge to 0.2 V	
Sample 3	discharge to 0.05 V	
Sample 4	discharge to 0.005 V	
Sample 5	discharge to 0.005 V and keep at 0.005 V for 48 h charge to 2 V	
Sample 6	discharge to 0.2 V	FEC-based electrolyte, RT
Sample 7	discharge to 0.05 V	
Sample 8	discharge to 0.005 V	
Sample 9	discharge to 0.005 V and keep at 0.005 V for 48 h	
Sample 10	charge to 2 V	
Sample 11	discharge to 0.005 V and keep at 0.005 V for 48 h	FEC-based electrolyte, 55 ℃
Sample 12	charge to 2 V	

2.4. Characterization

A Swageloke-type two-electrode cell was assembled in an Ar-filled glove box. The Si thin film was used as the working electrode, and a lithium foil as the counter electrode. After cycling, the cells were disassembled in the Ar-filled glove box, and the Si thin films were washed by DMC to remove residual of $LiPF_6$. The samples were then vacuum-dried for more than 5 h before AFM (MultiMode 8, Bruker, equipped inside an Ar glove box) study. A random 45 μm×45 μm area was selected on each sample and 225 force curves in total were obtained for each sample in the chosen area. The space distance between two force curves was 3 μm. As for the AFMFS measurement, a batch of flat Si thin film electrodes were prepared under the same condition by magnetron sputtering. Titanium was deposited on a polished quartz substrate by direct current magnetron sputtering to serve as the current collector. The Si film (∼ 410 nm in thickness) was then deposited on the titanium layer directly by radio frequency magnetron sputtering. The sputtering chamber was vacuumed to 2×10^{-4} Pa before depositing and was kept at 0.5 Pa under pure Ar (> 99.999%).

3. Results and discussion

Figure 1(a) shows the cycling performance of the cells containing the EC-based (50% EC) and the FEC-based (30% FEC) electrolytes. Excellent reversible capacities were observed for the cells containing either FEC or EC. The reversible capacity of the silicon electrode in the EC-based electrolyte was 3126 mA·h/g for the first cycle. The same electrode in the FEC-based electrolyte had an initial capacity of 3102 mA·h/g, slightly lower than that in the EC-based electrolyte. The Coulombic efficiency in the first cycle was 90% for the EC-based electrolyte while it was 86% for the FEC-based electrolyte (Figs. 1(b) and 1(c)). Furthermore, the cells containing FEC showed better cycling performance than those without FEC after 30 cycles.

In order to study the SEI film using AFMFS method, amorphous Si thin film electrodes (a-Si is used in the following text for convenience) were prepared by magnetron sputtering.[54] Figure 2(a) indicates the discharging and charging states of the a-Si electrodes. Figures 2(b)–2(g) show the surface morphology evolution. The top view of the pristine a-Si electrode displays spherical grains with the average grain size ranging from tens to hundreds of nanometers. The grain size increases gradually with the insertion of Li-ion during discharging and decreases slightly after charging. This can be shown clearly in the roughness statistics in Fig. 2(h). The roughness R_q is measured by root-mean-squared (RMS) values determined from the AFM images.[55] At the charging state, the cracking can also be seen.

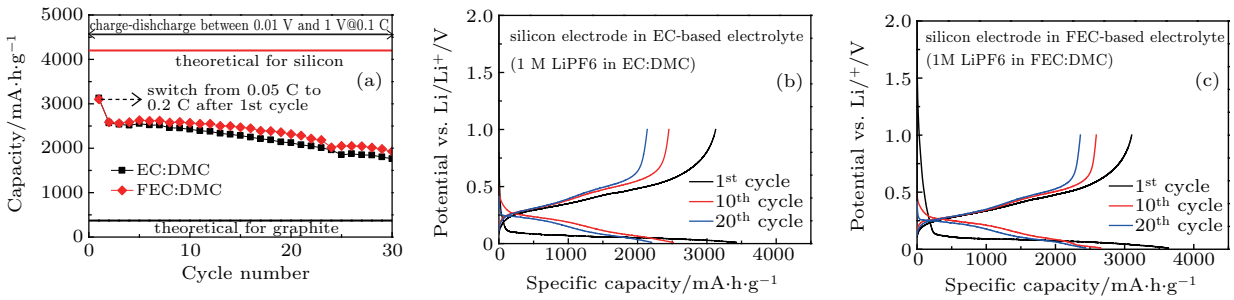


Fig. 1. (a) Reversible capacity of the silicon electrodes in the FEC-based electrolyte and the EC-based electrolyte. Charge and discharge curves of the silicon electrode cycled (b) in the EC-based electrolyte and (c) in the FEC-based electrolyte.

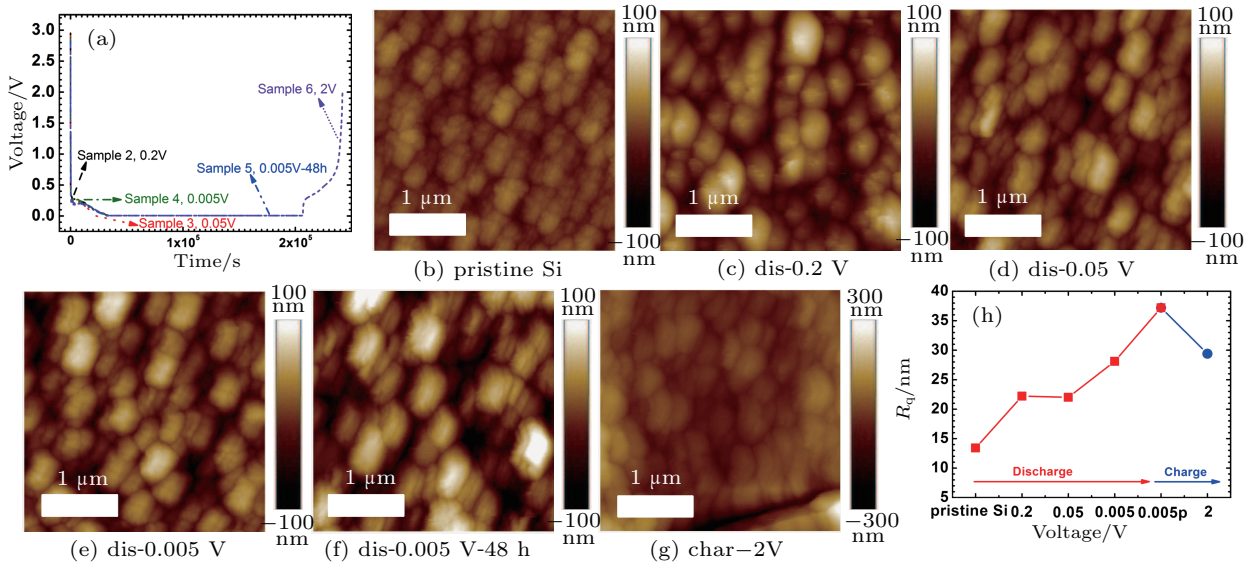


Fig. 2. (a) Voltage profile of samples 2–6, which were discharged to 0.2 V, 0.05 V, 0.005 V, 0.005 V (kept at 0.005 V for 48 h), and charged to 2 V. (b)–(g) Roughness of samples 1–6. (h) AFM topographical images (3 μm×3 μm) of samples 1–6, where sample 1 was the pristine Si thin film.

For a 45 μm×45 μm crack-free square region which was selected randomly, the AFM tip probed the force response every 3 μm. Total 225 force curves were collected for every sample. The diameter of the tip is about 4 nm (it is about 80 nm when the immersion depth of the tip is 100 nm). Therefore, we believe that the microstructure of neighbor spots will not influence each other by each probing. Five typical types of force curves have been obtained, as shown in Fig. 3, which could correspond to five different surface structures. Each layer has a set of elastic region and yield region. Normally, the elastic region has a linear slope while the slope of the yield region changes compared with that of the elastic region. This is the reason for the existence of several points of inflexion on a curve. Though the amplification of the first derivative between two layers is very small for the short indentation depth and similar composition, the second derivative has a huge change. So the multilayers can be distinguished from each other through the huge change of the second derivative. Figure 3(a) shows the force curve of the naked surface of the Li–Si alloy. The second type of force curve profile is shown in Fig. 3(c). In this figure, $\delta = 0$ (directed by the olive arrow) is the start-contact point of the tip and sample surface. So $\delta < 0$ means that the tip stays far enough from the sample, beyond the range of any tip–sample interactions. Then the tip is loaded towards to the surface of the sample. A set of elastic region ($0 < \delta < 50.89$ nm, a linear slope in the indentation curve) and yield region (50.89 nm $< \delta <$ 70.46 nm, the slope decreased compared with the elastic region) can be observed. Then a sharp increasing region appears above 70.46 nm, which is related to the Li–Si alloy (representative force curve of Li–Si is shown in Fig. 3(a)). It is supposed that the structure of the detected point is a single-layered SEI with the thickness of 70.46 nm, as drawn in Fig. 3(d) for reference. The third type of force curve profile has two sets of elastic, yield regions ($0 < \delta <$ 12.95 nm, 12.95 nm $< \delta <$ 44.05 nm) in one force curve, corresponding to a 12.95 nm layer and a 31.1 nm layer, respectively. We believe that this is related to a double-layer structure as described in Fig. 3(f). This type of double-layered force curve was also observed in the case of SEI on Cu anode in a Na battery. During the interaction process, the top soft layer of SEI could be compressed by the tip and a compact SEI formed, thus the force behavior of the compressed SEI was modified compared to the soft one.[50] The fourth type of force curve profile is composed of three regions as shown in Fig. 3(g), $0 < \delta <$ 20.75 nm for the first layer, 20.75 nm $< \delta <$ 42.84 nm for the second layer, and 42.84 nm $< \delta <$ 69.42 nm for the third layer. Each layer is identified by one set of elastic and yield regions. This could be an area with a triple-layered structure, as shown in Fig. 3(h). The fifth type of force curve is shown in Fig. 3(i). It increases to about 60 nN as the sample deformation is 13 nm and then decreases from 60 nN to 30 nN in the region of 13 nm $< \delta <$ 28 nm. This phenomenon means that the tip may touch a bubble existed in the SEI film. This is reasonable that some authors have proposed such possibility previously.[56,57] The bubble could generate since the reduction of the electrolyte will produce CO_2, CO, CH_4, C_2H_4, *et al.*[58] In some surface areas of the cycled Si thin film, none of the above four types of force curves are obtained. Compared to the fresh a-Si electrode, a linear response with relatively low slope can be found (see Fig. 3(a)). This area should be the naked lithiated a-Si surface. Based on the responses of the force curves in each detected point, we could judge easily whether the surface at that point is covered by the SEI or not, and whether the SEI is single layer or multiple layers.

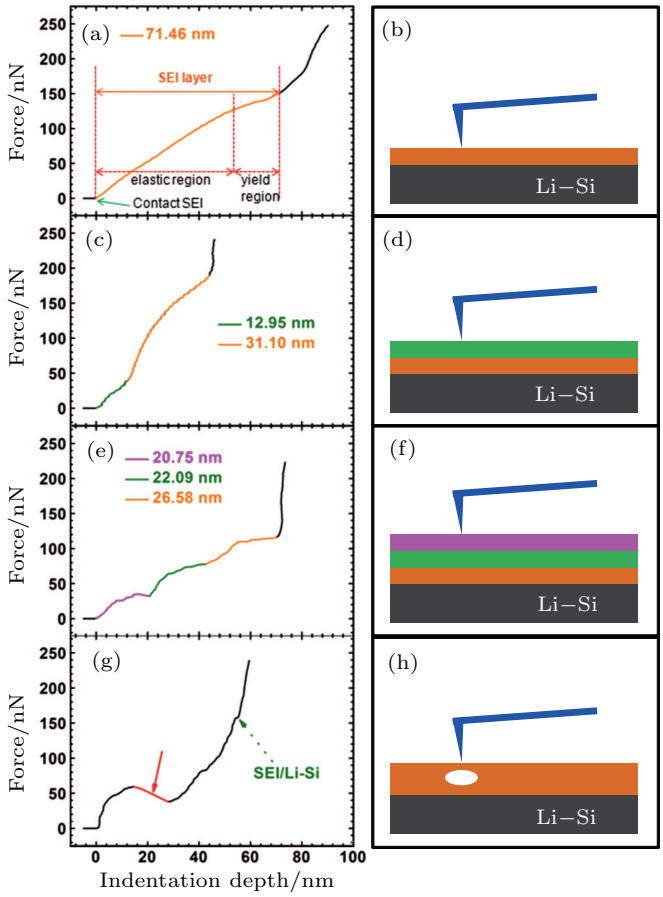


Fig. 3. Typical profiles of force curve spectroscopy: (a) naked surface of the Li–Si alloy after cycle, (c) single-layered SEI, (d) double-layered SEI, (g) triple-layered SEI, (i) bubble; (b) (d), (f), (h), (j) possible models for the previous structures.

As mentioned above, the thickness of each layer of the SEI film can be obtained from the force curves. The total SEI thickness statistics of the various samples at different states are shown in Fig. 4. The frequency of the Y axis means the number of the force curves with the feature of the SEI. The thickness means the total thickness of the SEI at certain point, whatever the SEI in that point is single layer or triple layer.

For the samples with EC-based electrolyte (Figs. 4(a)–4(d)), the area with SEI can be detected out only when the a-Si electrodes are discharged below 0.05 V. The number of thicker SEI areas increases gradually with decreasing the discharge voltage. The number of thicker SEI decreases after charging to 2.0 V. In the case using the FEC-contained electrolyte, the area with SEI can be detected out at a higher discharging cut-off voltage of 0.2 V. The general trend of the thickness variation of the SEI during discharging and charging is similar to that of the FEC-free samples (Figs. 4(e)–4(h) for discharging, Fig. 4(i) for charging). Relatively speaking, the number of the areas with thick SEI and the thickness of the a-Si electrode in the electrolyte with FEC are larger than those of the a-Si electrode in the FEC-free electrolyte.

The effect of temperature was also investigated. The a-Si electrodes were discharged at 55 ℃ and then charged after cooled down to room temperature for AFMFS testing. Obviously, the SEI grown at 55 ℃ is thinner than that at room temperature. It is supposed that part of the SEI could be more dissolvable at elevated temperature, which has been noticed previously.[7,43]

Young's modulus can be extracted from each force curve. During measurement, a conical type tip (tip radius ~ 2 nm) was inserted into a flat surface. The relationship among Young's modulus, sample deformation, and loading force can be described by the Sneddon model[59]

$$F = (2/\pi)(E/(1-\nu^2))\delta^2 \tan(\alpha), \tag{1}$$

where F is the loading force, E is the Young's modulus, δ is the sample deformation of the elastic region, α is the half

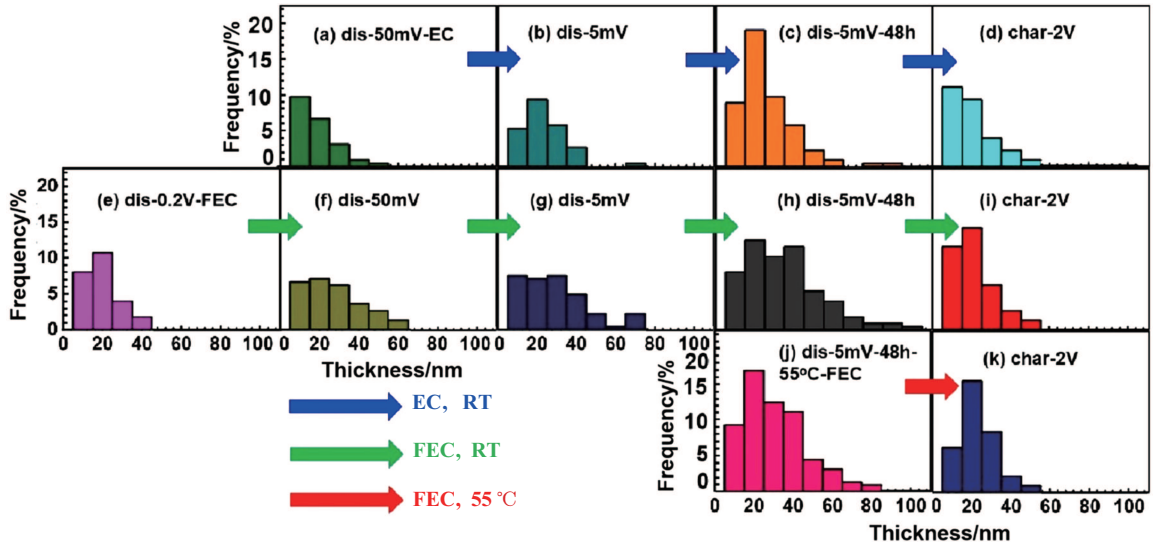


Fig. 4. Thickness distribution of SEI: (a)–(d) for samples 2–5 (blue arrow: discharged to 0.05 V, 0.005 V, 0.005 V and kept at 0.005 V for 48 h, charged to 2 V; EC-based electrolyte, RT), (e)–(i) for samples 6–10 (olive arrow: discharged to 0.2 V 0.05 V, 0.005 V, 0.005 V and kept at 0.005 V for 48 h, charged to 2 V; FEC-based electrolyte, RT), (j)–(k) for samples 11–12 (red arrow: discharged to 0.005 V and kept at 0.005 V for 48 h, charged to 2 V; FEC-based electrolyte, 55 ℃).

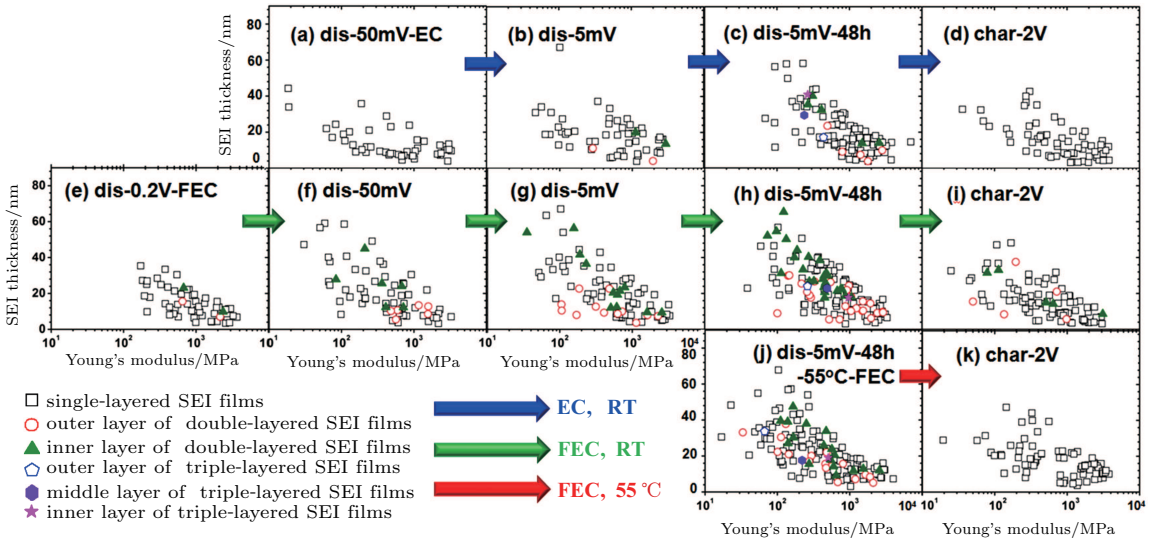


Fig. 5. Relation between SEI thickness and Young modulus: (a)–(d) for samples 2–5 (blue arrow: discharged to 0.05 V, 0.005 V, 0.005 V and kept at 0.005 V for 48 h, charged to 2 V; EC-based electrolyte, RT), (e)–(i) for samples 6–10 (olive arrow: discharged to 0.2 V 0.05 V, 0.005 V, 0.005 V and kept at 0.005 V for 48 h, charged to 2 V; FEC-based electrolyte, RT), (j)–(k) for samples 11–12 (red arrow, discharged to 0.005 V and kept at 0.005 V for 48 h, charged to 2 V; FEC-based electrolyte, 55 °C). Black square is for single-layered SEI films; red square and olive triangle are for the outer and inner layers of double-layered SEI films; blue square, violet triangle, and magenta pentagon are for the outer, middle, and inner layers of triple-layered SEI films, respectively.

angle of the conical tip ($\alpha = 20°$), ν is the Poisson ratio which was set to be 0.5, assuming rubber elasticity for the SEI films at the early stage of the elastic region of the force curve.[48,50] At the detected point, the information of the Young's modulus at each layer can be obtained. Since we have already obtained the information of the SEI thickness of each layer, we can draw a plot of Young's modulus versus the SEI thickness of each layer. In order to distinguish the SEI with different layer structure, the SEI areas with single layer, double layer, or triple layer are marked with different symbols. As shown in Figs. 5(a)–5(d), soft and hard SEI areas coexist once the SEI is formed after discharging to 50 mV. More soft SEI areas with low Young's modulus appear at deep discharging state, as shown in Fig. 5(c). The areas with single-layered structure have the highest probability to appear at all discharging and charging states. The SEI areas with double-layered structure appear after discharging to 0.005 V and the triple-layered structure appears after discharging at 5 mV and keeping potentiostatically for extra 48 h, as shown in Figs. 5(b) and 5(c). After charging, only single-layered SEI remains and more soft SEI areas disappear, as shown in Fig. 5(d).

The influence of the FEC on the mechanical properties of the formed SEI is shown in Figs. 5(e)–5(i). The most striking differences of a-Si electrodes in the FEC electrolyte and FEC-free electrolyte are noticed as follows.

1) The appearance of the SEI at 0.2 V for the FEC case, as shown in Fig. 5(e) (this is also observed in Fig. 4(e)), the start-formation potential of the EC-based electrolyte is 0.05 V. The Young's modulus of SEI at 0.2 V is at least larger than 100 MPa, most of areas are single layer and the thickness is less than 40 nm. The Young's modulus is below 100 MPa during the following discharging process, implying that the softer SEI formed under this condition could be mainly composed of organic layer.

2) The amount of double-layered and triple-layered SEI is relatively higher in the FEC case and increases with decreasing discharging voltage (Figs. 5(e)–5(i)).

3) The double-layered SEI areas remain even after charging to 2.0 V (Fig. 5(i)) in the FEC samples while only single-layered SEI remains in the EC ones (Fig. 6(d)), it means that the FEC, used as co-solvent of the electrolyte, is helpful to form the SEI with better structural and electrochemical stability.

At 55 °C, the general tendency is similar. Soft SEI areas disappear significantly after charging to 2.0 V. A slight difference is that the multi-layered SEI areas are fewer than that at room temperature for the fully discharged a-Si electrodes, as shown in Fig. 5(h). Comparing the a-Si electrodes after charging at 2.0 V at room temperature (Fig. 5(i)) and at 55 °C (Fig. 5(k)), both soft and hard SEI are much less at elevated temperature. This suggests further that the solubility of the SEI at elevated temperature is increased significantly, especially for the soft components.

At each AFMFS measured point in the scanned area, the Young's modulus can be obtained. If the SEI is single layer, one Young's modulus value at different indentation depth can be obtained. If the SEI is multi-layered, several Young's modulus values can be obtained. At each point, the thickness of the SEI for each layer is also known. Therefore, 3D plots can be drawn based on the above analysis, as shown in Fig. 6. The SEI is presented in the *xyz* coordinates, where *x* and *y* are the positions of each force curve in the 45 μm×45 μm surface and

z is the thickness of the SEI measured. The Young's modulus of the SEI is represented by the color bar ranging from 0 to 4 GPa. It can be seen that the surface of the a-Si electrodes at every state is not covered completely by the SEI film. Some areas are still naked even at deeply discharging state. The SEI on a-Si anode looks like a wild forest, distributed randomly and inhomogeneously. The SEI morphology on the silicon surface has been studied by Choi.[60] The lithium alloy with a particle-like shape is generated and the volume expands during the period of charging. When the lithium is removed from the alloy, the electrode shrinks and produces cracks. The cracking on the surface proceeds and the cracked silicon becomes smaller with cycle number. This can be attributed to the volumetric stresses of the insertion/extraction lithium of the lithium–silicon alloy during the repeated cycling. The FEC is helpful to the formation of SEI layer on the cracked surface of the electrode by reductive decomposition of the electrolyte solution. Conclusions drawn from Fig. 6 are the same as above analysis, obviously, the variation of the SEI morphology upon the discharging and charging, the effect of the FEC and temperature can be seen clearly and straightforwardly. Especially, the shell of the SEI is composed of soft SEI as shown by blue color with lower Young's modulus.

The projection of the 3D plots in Fig. 6 gives a 2D plot which will indicate the coverage of the SEI on the a-Si electrodes. Each 2D projection plot as shown in Figs. 7(a)–7(k) corresponds to the 3D plot in Fig. 6, respectively. From this figure, it is more obvious that many areas are in black color and not covered by the SEI film. From Fig. 7, the coverage can be calculated quantitatively by the following equation:

$$\text{coverage} = \frac{\text{number of force curves with SEI response}}{\text{total number of force curves}}. \quad (2)$$

The results are shown in Fig. 8. It is clearly that the SEI coverage increases continuously to 50% after discharging to 5 mV and decreases continuously to 30% after charging to 2.0 V with the EC-based electrolyte. The addition of FEC is beneficial to increasing the coverage of SEI to 60%. However, the SEI is not electrochemically stable, especially for the "soft" parts as mentioned above.

Full coverage of stable and homogeneous SEI on the surface of electrode in lithium ion batteries is desirable for achieving high Coulombic efficiency at successive cycles and long cycling life. The coverage of the SEI film could be influenced by many aspects leading to inhomogeneity, perhaps including the electronic conductivity of the electrodes, wetting effect of the electrolyte on the surface of the electrodes, ionic current distribution on the surface of the electrode, dynamic equilibrium between the deposition and dissolution of the SEI components, and surface energy of the electrodes. Up to now, the related knowledge is very poor. We could not explain clearly why the SEI cannot cover the surface of the a-Si thin film electrodes in all cases even after the a-Si electrodes are kept at 0.005 V for 48 h. Comprehensive investigations and comparisons on other material systems should be helpful for clear understanding.

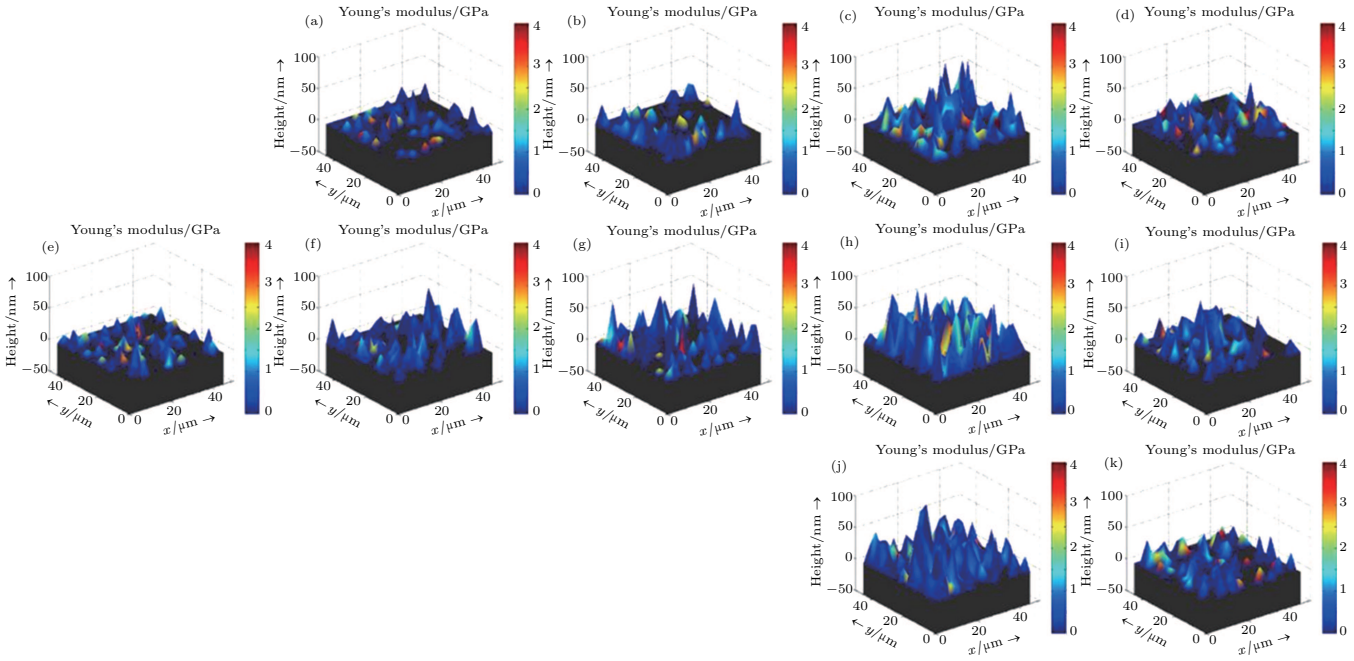


Fig. 6. Three-dimensional plots (a)–(d) for samples 2–5 (discharged to 0.05 V, 0.005 V, 0.005 V and kept at 0.005 V for 48 h, charged to 2 V; EC-based electrolyte, RT), (e)–(i) for samples 6–10 (discharged to 0.2 V 0.05 V, 0.005 V, 0.005 V and kept at 0.005 V for 48 h, charged to 2 V; FEC-based electrolyte, RT), (j)–(k) for samples 11–12 (red arrow, discharged to 0.005 V and kept at 0.005 V for 48 h, charged to 2 V; FEC-based electrolyte, 55 °C), Black substrates are for Li–Si alloy, x, y axes are the coordinates of the SEI film and z axis is the thickness of the SEI film. The color bar of 0–4 GPa is the Young's modulus for the SEI films.

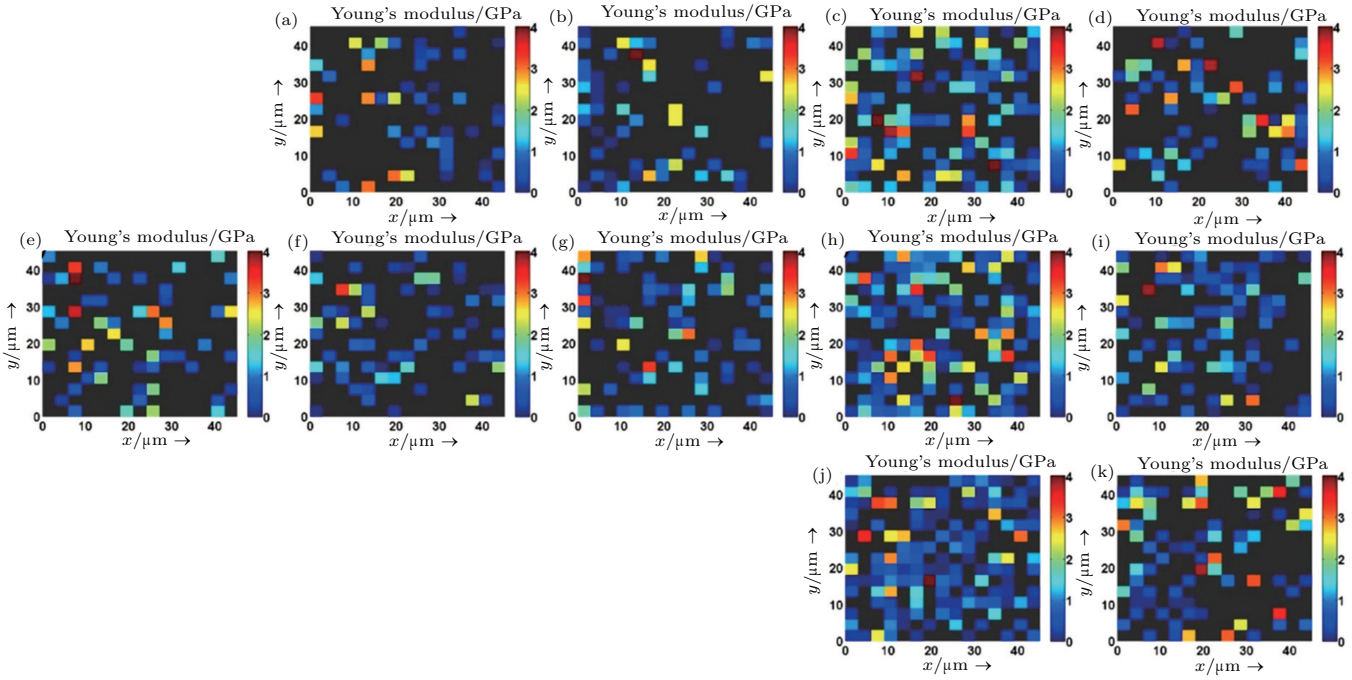


Fig. 7. (a)–(k) The 2D projection of 3D plots in Figs. 6(a)–6(k), respectively.

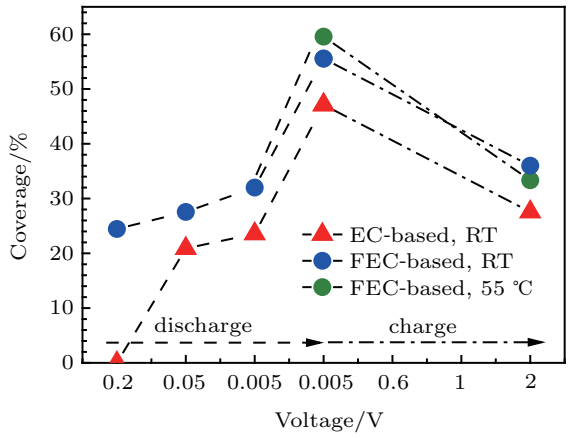


Fig. 8. SEI coverage (Eq. (2)) for samples 2–5 (EC-based electrolyte, RT), (e)–(i) samples 6–10 (FEC-based electrolyte, RT), and (j)–(k) samples 11–12 (FEC-based electrolyte, 55 ℃).

In spite of uncertainty of the mechanism, based on the above findings, we believe that *ex situ* AFMFS could be developed into a powerful tool for studying the SEI with complicated surface structure and can be very helpful for screening the electrolyte additives and studying the function of the polymer binder.

Actually, quantitative analysis based on *in situ* AFMFS measurements is more desired. However, all of our efforts have not been successful up to now due to the quick evaporation of the electrolytes in the glove box. Collecting 225 force curves needs two hours while the electrolyte on the surface of the a-Si electrode will be dried within 10 min. This problem could be solved by exchanging the volatile nonaqueous electrolyte into stable ionic liquid. It is certainly valuable but the important information of the SEI film formed in commonly used carbonate electrolytes cannot be obtained. Alternatively, high speed force curve scanning mode or hundreds tips AFM instruments could be developed for this purpose.

4. Conclusions

Ex situ scanning AFMFS method has been used to study the SEI film on a-Si thin film electrodes. By analyzing hundreds of force curves collected in certain area, the thickness distribution, multi-layered structure, Young's modulus, and the coverage of the SEI can be obtained. The 3D visualization of the SEI has been realized. It is found that the SEI grows thicker and softer during discharging. The soft parts tend to decompose during charging. Elevating operating temperature of the cell will lead to the dissolution of the SEI, especially for the soft parts. The FEC-contained electrolyte is beneficial to form the SEI film at higher discharge voltage and improve the SEI coverage, compared to the EC-based electrolyte. This could explain the enhancement effect of the FEC on the cyclic performance of the Si anode. Since this method could provide unique information, it is believed that the combination of the scanning AFMFS method with other techniques, such as SIMS, XPS, EELS, and ABF-STEM will be developed as a powerful tool kit to provide complete picture of the SEI with chemical, microstructure, and mechanical properties in future.

Acknowledgment

The scientific contributions from Dr. Hao Sun from Bruker Corporation are acknowledged here for the discussions about AFM experiments.

References

[1] Thackeray M M, Wolverton C and Isaacs E D 2012 *Energ. Envron. Sci.* **5** 7854
[2] Scrosati B, Hassoun J and Sun Y K 2011 *Energ. Envron. Sci.* **4** 3287
[3] Lu J, Chen Z, Ma Z, Pan F, Curtiss L A and Amine K 2016 *Nat. Nanotechnol.* **11** 1031
[4] Wang Y and Zhong W H 2015 *ChemElectroChem.* **2** 22
[5] Verma P, Maire P and Novák P 2010 *Electrochim. Acta* **55** 6332
[6] Jaguemont J, Boulon L and Dubé Y 2016 *Appl. Energy* **164** 99
[7] Aravindan V, Lee Y S and Madhavi S 2017 *Adv. Energy. Mater.* **7** 1602607
[8] Li W, Song B and Manthiram A 2017 *Chem. Soc. Rev.* **46** 3006
[9] Ding Y, Mu D, Wu B, Wang R, Zhao Z and Wu F 2017 *Appl. Energy* **195** 586
[10] Schulz N, Hausbrand R, Wittich C, Dimesso L and Jaegermann W 2018 *J. Electrochem. Soc.* **165** A833
[11] Morales U J E, Bolimowska E, Rouault H, Santos Peña J, Santini C C and Benayad A 2018 *J. Phys. Chem. C* **122** 18223
[12] Sun H H, Dolocan A, Weeks J A, Rodriguez R, Heller A and Mullins C B 2019 *J. Mater. Chem. A* **7** 17782
[13] Peled E and Menkin S 2017 *J. Electrochem. Soc.* **164** A1703
[14] Yoon T, Milien M S, Parimalam B S and Lucht B L 2017 *Chem. Mater* **29** 3237
[15] Franco A A, Rucci A, Brandell D, Frayret C, Gaberscek M, Jankowski P and Johansson P 2019 *Chem. Rev.* **119** 4569
[16] Li H, Huang X, Chen L, Wu Z and Liang Y 1999 *Electrochem. Solid State Lett.* **2** 547
[17] Li H, Huang X, Chen L, Zhou G, Zhang Z, Yu D, Mo Y J and Pei N 2000 *Solid State Ion* **135** 181
[18] Zhang C, Gu L, Kaskhedikar N, Cui G and Maier 2013 *J ACS Appl. Mater. Interfaces* **5** 12340
[19] Ling M, Xu Y, Zhao H, Gu X, Qiu J, Li S, Wu M, Song X, Yan C and Liu G 2015 *Nano Energy* **12** 178
[20] Jin Y, Zhu B, Lu Z, Liu N and Zhu J 2017 *Adv. Energy Mater.* **7** 1700715
[21] Zhou X, Chen J, Gu L and Miao L 2015 *Chin. Phys. Lett.* **32** 026102
[22] Xu H, Zhang H, Ma J, Xu G, Dong T, Chen J and Cui G 2019 *ACS Energy Lett.* **4** 2871
[23] Chan C, Ruffo R, Hong S S and Cui Y 2009 *J. Power. Sources* **189** 1132
[24] Dupré N, Moreau P, De Vito E, Quazuguel L, Boniface M, Bordes A, Rudisch C, Bayle G P and Guyomard D 2016 *Chem. Mater* **28** 2557
[25] Wang C, Ouyang L, Fan W, Liu J, Yang L, Yu L and Zhu M 2019 *J. Alloys Compd.* **805** 757
[26] Wang J, Zhang L and Zhang H 2018 *Ionics* **24** 3691
[27] Wang W and Yang S 2017 *J. Alloys Compd.* **695** 3249
[28] Jo H, Kim J, Nguyen D T, Kang K K, Jeon D M, Yang A R and Song S W 2016 *J. Phys. Chem. C* **120** 22466
[29] Nguyen C C and Lucht B L 2018 *J. Electrochem. Soc.* **165** A2154
[30] Li Q, Liu X, Han X, Xiang Y, Zhong G, Wang J, Zheng B, Zhou J and Yang Y 2019 *ACS Appl. Mater. Interfaces* **11** 14066
[31] Jaumann T, Balach J, Langklotz U, Sauchuk V, Fritsch M, Michaelis A, Teltevskij V, Mikhailova D, Oswald S and Klose M 2017 *Energy Storage Mater.* **6** 26
[32] Srivastav S, Xu C, Edström K, Gustafsson T and Brandell D 2017 *Electrochim. Acta* **258** 755
[33] Lindgren F, Xu C, Niedzicki L, Marcinek M, Gustafsson T, Björefors F, Edström K and Younesi R 2016 *ACS Appl. Mater. Interfaces* **8** 15758
[34] Schroder K, Alvarado J, Yersak T A, Li J, Dudney N, Webb L J, Meng Y S and Stevenson K J 2015 *Chem. Mater.* **27** 5531
[35] Wu C J, Rath P C, Patra J, Bresser D, Passerini S, Umesh B, Dong Q, Lee T C and Chang J K 2019 *ACS Appl. Mater. Interfaces* **11** 42049
[36] Erickson E M, Markevich E, Salitra G, Sharon D, Hirshberg D, de la Llave E, Shterenberg I, Rosenman A, Frimer A and Aurbach D 2015 *J. Electrochem. Soc.* **162** A2424
[37] Xu Z, Yang J, Li H, Nuli Y and Wang J 2019 *J. Mater. Chem. A* **7** 9432
[38] Yao K, Zheng J P and Liang R 2018 *J. Power. Sources* **381** 164
[39] Dunn R P, Nguyen C C and Lucht B L 2015 *J. Appl. Electrochem* **45** 873
[40] Men F, Yang Y, Shang Y, Zhang H, Song Z, Zhou Y, Zhou X and Zhan H 2018 *J. Power. Sources* **401** 354
[41] Ababtain K, Babu G, Lin X, Rodrigues M T F, Gullapalli H, Ajayan P M, Grinstaff M W and Arava L M R 2016 *ACS Appl. Mater. Interfaces* **8** 15242
[42] Aurbach D, Zaban A, Ein E Y, Weissman I, Chusid O, Markovsky B, Levi M, Levi E, Schechter A and Granot E 1997 *J. Power. Sources* **68** 91
[43] Alliata D, Kötz R, Novák P and Siegenthaler H 2000 *Electrochem. Commun.* **2** 436
[44] Chu A C, Josefowicz J Y and Farrington G C 1997 *J. Electrochem. Soc.* **144** 4161
[45] Jeong S K, Inaba M, Iriyama Y, Abe T and Ogumi Z 2003 *J. Power. Sources* **119–121** 555
[46] Inaba M, Tomiyasu H, Tasaka A, Jeong S K and Ogumi Z 2004 *Langmui* **20** 1348
[47] Luo F, Chu G, Xia X, Liu B, Zheng J, Li J, Li H, Gu C and Chen L 2015 *Nanoscale* **7** 7651
[48] Becker C R, Strawhecker K E, McAllister Q P and Lundgren C A 2013 *Acs. Nano* **7** 9173
[49] Beaulieu L Y, Hatchard T D, Bonakdarpour A, Fleischauer M D and Dahn J R 2003 *J. Electrochem. Soc.* **150** A1457
[50] Wang Y H, He Y, Xiao R J, Li H, Aifantis K E and Huang X J 2012 *J. Power. Sources* **202** 236
[51] Zhang J, Yang X, Wang R, Dong W, Lu W, Wu X, Wang X, Li H and Chen L 2014 *J. Phys. Chem. C* **118** 20756
[52] Hu X, Chan N, Martini A and Egberts P 2017 *Nanotechnology* **28** 025702
[53] Han M, Zhu C, Ma T, Pan Z, Tao Z and Chen J 2018 *Chem. Commun.* **54** 2381
[54] He Y, Yu X, Li G, Wang R, Li H, Wang Y, Gao H and Huang X 2012 *J. Power. Sources* **216** 131
[55] Lee H, Shin W, Choi J W and Park J Y 2012 *J. Phys. D* **45** 275301
[56] La Mantia F and Novák P 2008 *Electrochem. Solid State Lett.* **11** 84
[57] Kircheva N, Genies S, Brun-Buisson D and Thivel P X 2011 *J. Electrochem. Soc.* **159** A18
[58] Shin J S, Han C H, Jung U H, Lee S I, Kim H J and Kim K 2002 *J. Power. Sources* **109** 47
[59] Domke J and Radmacher M 1998 *Langmuir* **14** 3320
[60] Choi N S, Yew K H, Lee K Y, Sung M, Kim H and Kim S S 2006 *J. Power. Sources* **161** 1254